THE JOURNAL OF PHYSICAL CHEMISTRY LETTERS
A JOURNAL OF THE AMERICAN CHEMICAL SOCIETY

pubs.acs.org/JPCL Letter

Concerted Double Hydrogen-Bond Breaking by Intermolecular Coulombic Decay in the Formic Acid Dimer

Jiaqi Zhou, Shaokui Jia, Anna D. Skitnevskaya, Enliang Wang, Theresa Hähnel, Emma K. Grigoricheva, Xiaorui Xue, Jian-Xing Li, Alexander I. Kuleff, Alexander Dorn, and Xueguang Ren*

Cite This: *J. Phys. Chem. Lett.* 2022, 13, 4272−4279 Read Online

ABSTRACT: Hydrogen bonds are ubiquitous in nature and of fundamental importance to the chemical and physical properties of molecular systems in the condensed phase. Nevertheless, our understanding of the structural and dynamical properties of hydrogen-bonded complexes in particular in electronic excited states remains very incomplete. Here, by using formic acid (FA) dimer as a prototype of DNA base pair, we investigate the ultrafast decay process initiated by removal of an electron from the inner-valence shell of the molecule upon electron-beam irradiation. Through fragment-ion and electron coincident momentum measurements and *ab initio* calculations, we find that de-excitation of an outer-valence electron at the same site can initiate ultrafast energy transfer to the neighboring molecule, which is in turn ionized through the emission of low-energy electrons. Our study reveals a concerted breaking of double hydrogen-bond in the dimer initiated by the ultrafast molecular rotations of two FA^+ cations following this nonlocal decay mechanism.

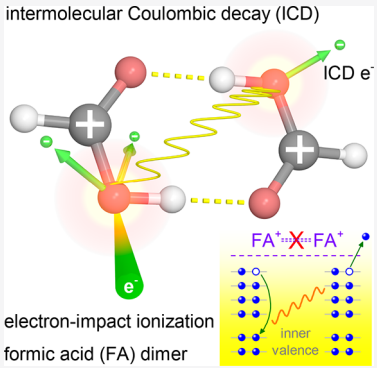

Intermolecular hydrogen bonds are essential in many areas of chemistry and biology and govern the properties and dynamics of molecular complexes at the microscopic level.[1−5] For example, they are the major intermolecular interactions in the liquid and solid structure of water and determine the stability and function of protein and DNA. In the double-stranded DNA, the adenine−thymine and guanine−cytosine base pairs are held together through double and triple hydrogen-bonds, respectively; if these hydrogen bonds are disrupted, it may cause DNA damage. As a result, studying the hydrogen bonds in the dimers or small clusters of molecules has become a subject of great interest for understanding the fundamental features of these intermolecular bonds.[6−9] In particular, there has been intense research on the hydrogen-bonding dimer of organic formic acid (FA, HCOOH) that is the smallest carboxylic acid and occurs naturally. In the formic acid dimer (FAD), the carboxylic oxygen of each unit is weakly bound to the acidic proton of the other unit via a hydrogen-bond, forming an eight-membered ring structure (Figure 1a), which can be regarded as a prototype system for studying the structures and dynamics of hydrogen-bonded base pairs.[10−17]

In recent years, investigations on the property of excited states in weakly bound systems are attracting considerable interest due to the discovery of a wealth of intermolecular relaxation processes. It was shown that the environment of a molecule with an inner-valence vacancy can actively take part in its de-excitation, giving rise to an ultrafast relaxation mechanism, predicted by Cederbaum et al. in 1997 and termed intermolecular Coulombic decay (ICD).[18] In ICD, the inner-valence vacancy is filled by an electron from an outer shell and the energy released is transferred to a neighboring molecule, which is in turn ionized through the emission of a low-energy electron. This nonlocal decay mechanism is ultrafast and evolves usually on a femtosecond time scale.[19−21] It results in the formation of two positive ions, leading typically to a Coulomb explosion of the system.

Experiments on ICD occurring after a manifold of excitation schemes have been identified in numerous systems,[22,23] such as van der Waals clusters,[24−28] hydrogen-bonded systems,[29−33] endohedral fullerenes,[34] helium droplets,[35] benzene dimers,[36] liquid water,[37,38] and condensed-phase interfaces.[39] The secondary ICD electrons usually have kinetic energies less than 10 eV and therefore have the capability to efficiently damage chemical bonds of neighboring molecules. Due to this key feature, ICD is expected to be a serious cause of DNA damage. Recent investigations on the hydrated biomolecules, where water is linked to biochemically relevant molecules via a hydrogen bond, imply that ICD can cause damage of biosystems directly by ionization.[32,33] Therefore, studying this mechanism in multiple hydrogen-bond systems would be of fundamental importance for understanding DNA damage at the molecular level.

Received: April 2, 2022
Accepted: May 3, 2022

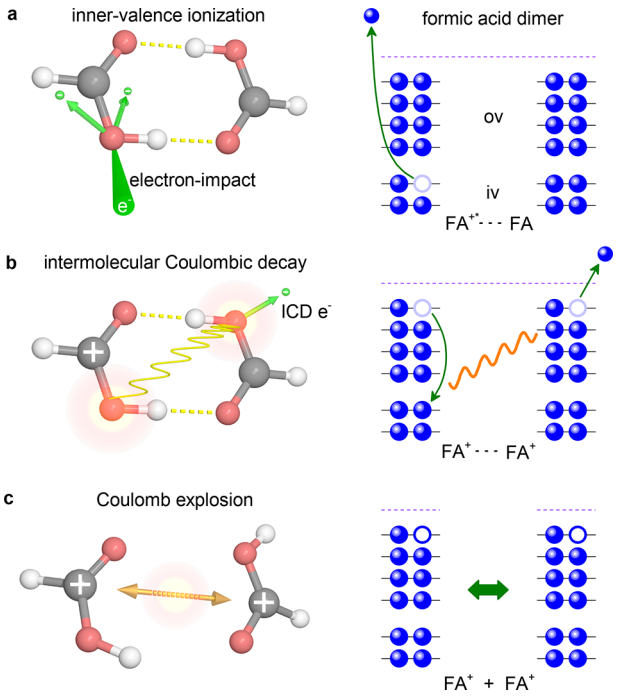

Figure 1. Illustration of ICD process in a double hydrogen-bonded formic acid dimer. (a) The ICD process is initiated by an inner-valence (iv) ionization of one of the FA molecules in the dimer. (b) The created iv vacancy is filled by an electron from the outer-valence (ov) shell at this site, and the energy released is transferred to the neighboring site from where a secondary low-energy electron is emitted. (c) Final fragmentation processes of the $FA^+\cdots FA^+$ dicationic dimer with a Coulomb explosion pathway.

In the present work, we report experimental evidence of ICD in FAD initiated by electron impact (E_0 = 90 eV). Here, the electron-initiated processes were thought to be responsible for an essential part of the radiation effects in gases and condensed matter.[40−42] Below we study this decay process through fragment ion and electron coincident momentum spectroscopy, accompanied by high-level electronic structure calculations[32] and *ab initio* molecular dynamics (AIMD) simulations. This would allow us to unambiguously identify the ionization mechanisms and elucidate the fragmentation dynamics of the $FA^+\cdots FA^+$ dicationic dimer. Experiments were carried out using a multiparticle imaging spectrometer (reaction microscope) combined with a pulsed photoemission electron source.[43−45] Our AIMD simulations of the $FA^+\cdots FA^+$ dication were performed based on the Born−Oppenheimer approximation in which six different isomers of neutral FAD are considered[46] (see Methods).

We have computed the double ionization threshold of FAD, which amounts to 28.45 eV at the EOM-DIP-CCSD/cc-pVTZ level (see Methods). This corresponds to single ionization of both molecules within the dimer and is thus attributed to the ICD final state. Previous studies of the inner-valence ionization spectra of FA molecule[47−50] have shown that the carbon 2s (C 2s) type states contribute mainly to the ionization-energy region of about 20−28 eV, while the ionization bands above 28 eV are mostly built on oxygen 2s (O2s) type states, i.e., the 5a′ and 4a′ orbitals. Hence, these states are energetically accessible for initiating the ICD process in FAD. More details will be provided in the following section. Here, the ionization and decay process is started by removal of an electron from the O2s inner-valence shell of FA molecule upon electron impact (Figure 1a). Afterward the $FA^{+*}(O2s^{-1})\cdots FA$ dimer cation undergoes ICD, i.e., an electron from higher-lying orbital of $FA^{+*}(O2s^{-1})$ fills the O2s vacancy, and an electron from the neighboring FA molecule is ejected, forming the $FA^+\cdots FA^+$ dicationic dimer (Figure 1b). The repulsion between the two positive charges leads to Coulomb explosion (CE) of the system (Figure 1c). The present study aims to understand the mechanistic details of double hydrogen-bond breaking in FAD following ICD.

In our experiments, two fragment ions and one of the three outgoing electrons are detected in triple coincidence such that during offline analysis, the mass-over-charge ratios, the momentum vectors, and the kinetic energies for three charged particles are determined (see Methods). We identify the dimer breakup channels using a time-correlation map which is shown in Figure 2. After the ionization and decay process the dimer

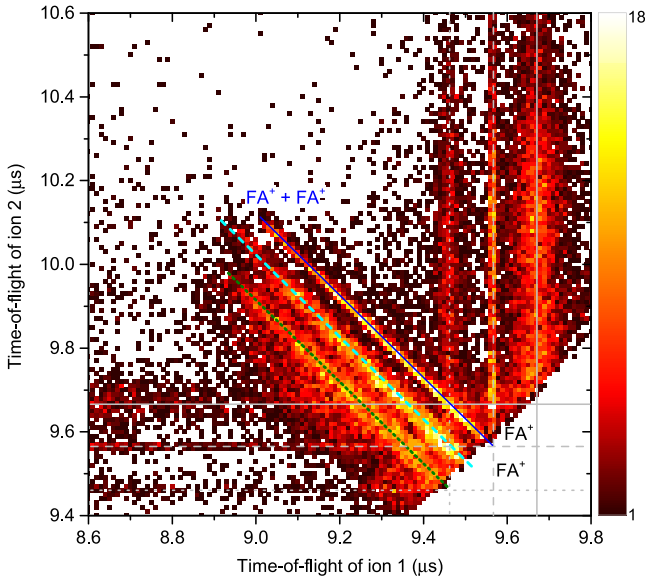

Figure 2. Correlation of the time-of-flight (TOF) of the two measured cations. The distributions at the solid, dashed, and dotted diagonal lines show the breakup of the dicationic dimer into FA^+ + FA^+, FA^+ + $[FA - H]^+$ + H, and $[FA - H]^+$ + $[FA - H]^+$ + 2H channels, respectively. The vertical and the horizontal dotted, dashed and solid lines represent the TOF of $[FA - H]^+$, FA^+, and $[FA + H]^+$ ions, respectively. The counts intensity is color-coded on a linear scale with a color bar shown on the right.

fragments into two singly charged ions which are emitted back-to-back with momenta of equal magnitude but opposite direction. As the time-of-flight (TOF) of an ion depends on its momentum and mass, the back-to-back emission leads to a diagonal line structure in the time-correlation map of both particles. The solid diagonal line indicates the position of events due to direct two-body fragmentation (FA^+ + FA^+). The dashed and dotted diagonal lines indicate the breakup channels where FA^+ emitted a neutral hydrogen atom, i.e., FA^+ + $[FA - H]^+$ + H (dashed line), and double hydrogen-loss $[FA - H]^+$ + $[FA - H]^+$ + 2H (dotted line). The correlation lines become broader for these hydrogen-loss channels due to the missing momenta of the undetected neutral species.

In the following, we discuss only the FA^+ + FA^+ CE channel that appears as the solid diagonal line in Figure 2 and can clearly be assigned to ionization and two-body fragmentation

https://doi.org/10.1021/acs.jpclett.2c00957
J. Phys. Chem. Lett. 2022, 13, 4272−4279

of the dimers. We first evaluate the spectra of emitted electrons recorded in coincidence with the FA^+ + FA^+ ion pair to show that ICD actually occurs for this fragmentation channel. The measurements of the scattered electrons allow us to determine the initial state of the decay process using the projectile energy loss (E_{loss}), as shown in Figure 3a,b, which is obtained by the

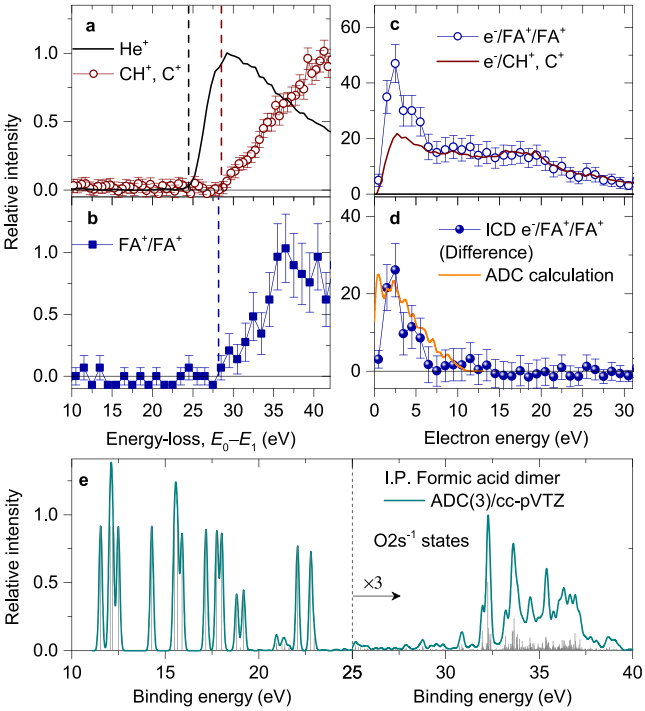

Figure 3. Measured and calculated energy spectra. (a) Projectile energy loss spectra for the inner-valence ionization of formic acid monomer that forms CH^+ and C^+ ions and for He(1s) ionization (solid line). (b) Energy loss spectrum for the double ionization of formic acid dimer leading to FA^+ + FA^+ ion pair. (c) Kinetic energy distributions of the emitted electrons for inner-valence ionization of FA monomer (solid line) and for ionization and fragmentation of FAD into FA^+ + FA^+. The spectra were normalized to each other in the energy range from 20 to 30 eV. (d) Difference spectrum obtained by subtracting the electron energy distribution of the monomer from the dimer shown in (c) and also ADC calculation[32] (solid line). (e) Calculated single-ionization spectrum of the FAD. Note that a different intensity scale is used between 25 and 40 eV.

incident electron energy (E_0) minus the energy of the scattered projectile (E_1). The minimum energy leading to specific ionization channels can be determined from the onsets of the E_{loss} spectrum, e.g., the E_{loss} of about 24.5 eV is obtained for the ionization of helium (He^+); see the solid line in Figure 3a, which is measured for the energy calibration of the experimental spectra. Also included in Figure 3a is the E_{loss} spectrum corresponding to the inner-valence ionization of the FA monomer, which can result in the CH^+ and C^+ products with an E_{loss} of about 28.5 eV. The measured E_{loss} spectrum for the FA^+ + FA^+ fragmentation channel is presented in Figure 3b. This spectrum shows an onset at E_{loss} ∼ 28.0−28.5 eV in agreement with our EOM-DIP-CCSD calculations, which lie in the range of the inner-valence ionization energies of 5a′ and 4a′ molecular orbitals.[47−50] Figure 3e presents the single-ionization spectrum of FAD computed at ADC(3)/cc-pVTZ level (see Methods). It reveals that the removal of an O2s electron leads to the population of a large number of states that lie above the double-ionization threshold of FAD (∼28.0 eV). These states, spread over nearly 10 eV (see the zoomed-in part of the spectrum above 25 eV in Figure 3e), can all further decay by emitting an electron from the neighboring FA molecule in an ICD process.

The ICD electrons are identified in Figure 3c,d which show the electron energy spectra up to 30 eV measured in coincidence with the FA^+ + FA^+ ion pair. The ICD electron emitted in Figure 1b cannot be seen separately since the spectrum contains background contribution of slow electrons arising from the initial direct electron-impact ionization process; see Figure 1a. In order to reveal the pure ICD electron spectra, we consider the electron energy spectrum for the inner-valence ionization of FA molecule as a reference (solid line) where ICD is absent, i.e., the spectrum corresponding to the CH^+ and C^+ products. This spectrum is normalized individually to the result of the dimer in the energy range above 20 eV where no ICD electrons contribute; see Figure 3c. An enhanced production of low-energy electrons is clearly observed in the spectrum of the dimer compared with the result of the monomer.[27,45] The difference, as shown in Figure 3d, is the pure ICD electron energy spectrum for the FA^+ + FA^+ CE channel. This spectrum shows a kinetic energy peak at about 2.5 eV with an energy range up to about 7 eV. The energy range of this spectrum is consistent with our calculations, which show a broad band for the binding energies of the $O2s^{-1}$ states mainly located at 30−40 eV (Figure 3e and Figure 1 of the Supporting Information). The lowest doubly ionized state of the FA molecule lies at about 33.24 eV, which is computed at the EOM-DIP-CCSD/cc-pVTZ level. This means that the states whose binding energies are higher than 33 eV may also relax through intramolecular Auger decay and form a FA^{++}···FA.[32] These results indicate that the singly ionized states lying at 28−33 eV are energetically accessible for the ICD channel in FAD, and thus, the ICD electron kinetic energies up to roughly 5 eV are expected for the FA^+ + FA^+ CE channel. Furthermore, we performed calculations for the ICD electron spectrum (solid line in Figure 3d) using the approach described in ref 32 (see Figure 3 of the Supporting Information), which is in good agreement with the experimental result. We note that a low-energy peak (<2.0 eV) of the ICD electron spectrum is not seen in the measurements as the efficiency of the electron spectrometer quickly drops at this energy range.[33,43]

In addition, as the obtained E_{loss} for FA^+ + FA^+ ion pair is close to the double ionization threshold of FAD, one may expect that another fragmentation pathway, namely, sequential ionization (where the projectile electron successively kicks out one electron from each molecule of the dimer and thus leads to the repulsive FA^+ + FA^+ ion pair), can contribute to this CE channel. Our analysis on the absolute cross section, however, indicates that the sequential ionization is only a minor channel[33] due to its low cross section (see Methods).

The measured kinetic energy release (KER) spectrum for the FA^+ + FA^+ CE channel is presented in Figure 4a which shows a single-peak structure centered at KER ∼ 4.15 eV. As the intermolecular potential drops with $1/R$ assuming two point-like charges separated by the distance R, we may deduce the Coulomb energy by considering that the two charges are located at the center-of-mass (COM) of the molecules. For a planar eight-membered ring structure of FAD (as shown in the inset in Figure 4a), which is suggested to be the lowest-energy configuration,[46] we determine the intermolecular COM

https://doi.org/10.1021/acs.jpclett.2c00957
J. Phys. Chem. Lett. 2022, 13, 4272−4279

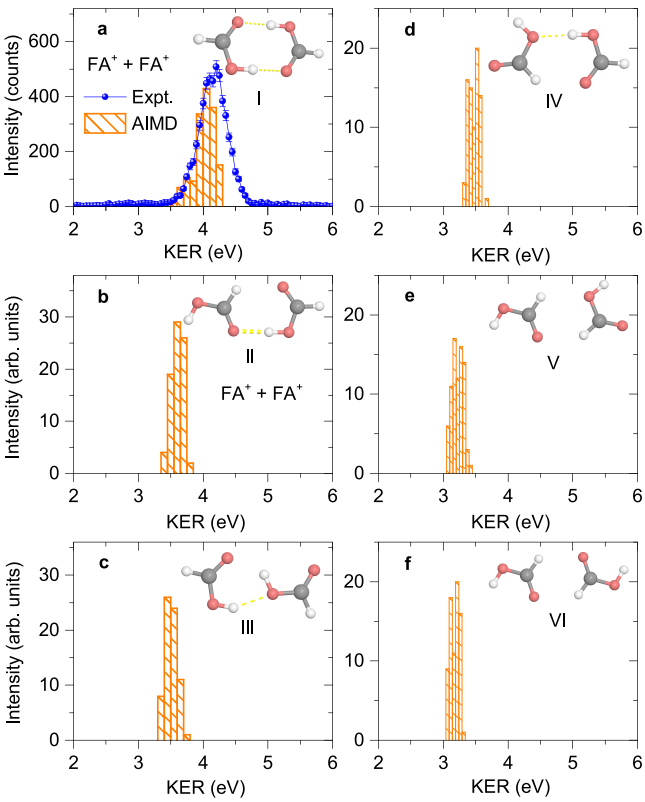

Figure 4. Kinetic energy release (KER) spectra of $FA^+ + FA^+$ ion pair. (a) Measured and *ab initio* molecular dynamics (AIMD) simulated KER spectra. Here, a planar eight-membered ring structure of FAD, corresponding to the global energy minimum geometry, was considered in the simulations. (b−f) AIMD simulated KER spectra corresponding to the isomers II−VI of FAD, respectively. The insets show the molecular geometries of different isomers of neutral FAD.[46]

distance (R_{COM}) of about 3.03 Å. This corresponds to KER ∼ 4.75 eV for the complete fragmentation of the dimer into an $FA^+ + FA^+$ ion pair, which is about 0.6 eV higher than the measured KER value.

To quantify this CE process, we have performed AIMD simulations starting from the sampled neutral dimers with a given initial temperature (30 K) and instantaneous removal of the two outermost electrons from each of the molecules. This means that the simulations are started from the final state of ICD, i.e., $FA^+\cdots FA^+$, corresponding to the electronic ground state of the dicationic dimer. We calculated the fragmentation dynamics of six different isomers of the neutral FAD[46] using the atom-centered density matrix propagation (ADMP) method with the long-ranged density-functional theory at the ωB97XD/cc-pVTZ level, which takes into account the internal and the rotational dynamics of the fragments (see Methods).

In the calculations, the KER value for each single trajectory is obtained by adding the Coulomb energy corresponding to the R_{COM} at t = 500 fs, which amounts to R_{COM} ∼ 43 au, to the KER resulting from the trajectory propagation.[51,52] As shown in Figure 4a, the calculated KER considering a planar eight-membered ring structure of neutral FAD reproduces very well the experimental spectrum. We note that the present simulations assume an instantaneous ICD decay, neglecting the molecular dynamics of the singly ionized $FA^{+*}(O2s^{-1})\cdots$ FA dimer before the onset of ICD and the decay to the doubly ionized $FA^+\cdots FA^+$ state. This may cause the slight deviations between calculated and measured KER in peak position (∼0.1 eV) and the narrow peak width of the calculated KER spectrum. The calculated KER distributions for II−VI isomers are presented in Figures 4b−f, respectively, which show single-peak structures centered at around 3.2−3.6 eV. The molecular structures for different isomers are also presented in the insets of Figure 4. These values are at least 0.5 eV smaller than the experimental and calculated KER shown in Figure 4a. This confirms the predominance of a planar eight-membered ring structure of the neutral FAD[46] in the present supersonic gas experiment. To estimate the part of energy that is transferred to internal and rotational motion of the fragments during the Coulomb explosion, we calculated the initial Coulomb energy (iCE) at t = 0, which corresponds to the Coulomb repulsion energy at R_{COM}, and assumed that all this energy is then entirely released as translational kinetic energy of the fragments. The results are shown in Figure 2 of the Supporting Information. The iCE spectrum corresponding to the planner eight-member ring isomer shows a peak at higher KER (∼4.75 eV), indicating that the amount of Coulomb energy deposited into internal and rotational energy of the two FA^+ fragments is roughly 0.7 eV.

To uncover the underlying dynamics of the present CE channel, we obtain the detailed temporal evolutions of the $FA^+\cdots FA^+$ dications with the predominant structure of FAD, which are presented in Figure 5. These results allow us to

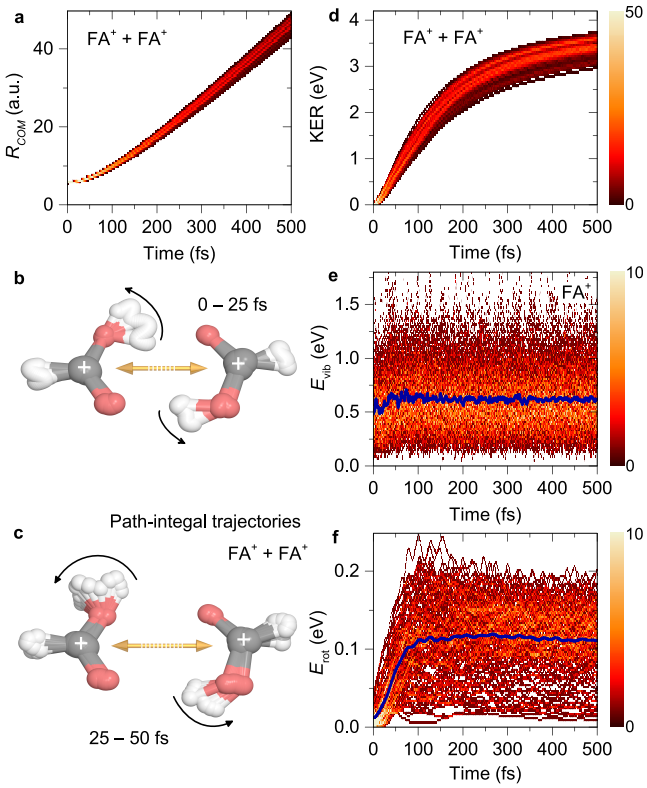

Figure 5. Fragmentation dynamics of the dicationic dimer into $FA^+ + FA^+$ pathway. (a) AIMD simulated center-of-mass (COM) distance (R_{COM}) between two FA^+ cations as a function of propagation time. (b, c) Path-integral trajectories in the time range of 0−25 fs (b) and 25−50 fs (c). (d−f) AIMD simulated KER of $FA^+ + FA^+$ ion pair (d) and vibrational energy E_{vib} (e) and rotational energy E_{rot} (f) of FA^+ cations as a function of time. The mean values for E_{vib} and E_{rot} are shown by the solid lines in (e) and (f), respectively. The color bar is linear with arbitrary units.

https://doi.org/10.1021/acs.jpclett.2c00957
J. Phys. Chem. Lett. 2022, 13, 4272−4279

elucidate the mechanistic details responsible for the double hydrogen-bond breaking and how the energy is distributed among the translational, vibrational, and rotational degrees of freedom of the two FA^+ molecular cations during the explosion. It can be seen from Figure 5a and Figure 5d that after the decay process the two FA^+ ions fly apart rapidly under the Coulomb repulsive force, i.e., both R_{COM} and KER of the $FA^+ + FA^+$ ion pair are starting to increase once ICD occurs.

The vibrational and rotational motions of fragments are investigated by deducing the vibrational and rotational energies for each of the FA^+ cations from the AIMD simulations.[51,52] The vibrational energy (E_{vib}) of FA^+ is presented in Figure 5e as a function of time, which shows a constant energy-spread evolution centered at $E_{vib} \sim 0.53$ eV over the whole range of propagation time (0−500 fs), indicating that the partitioning of KER and vibrational energy in the molecular fragments is determined early in the CE such that the total vibrational energy is constant over these time scales. While for the rotational energy (E_{rot}) of FA^+, shown in Figure 5f, we observe a fast increase of E_{rot}, due to the intermolecular Coulomb force, that converges to a constant value (∼125 meV) at larger time (>100 fs). This increased rotational frequency would cause the hydrogen-bond breaking of the system. It can be seen from the path-integral trajectories (0−50 fs) of the $FA^+ + FA^+$ ion pair, shown in Figure 5b,c, that the two hydrogens involved in the hydrogen bonding rotate very quickly out of the coplanar ring of the dimer. This leads to a fast and concerted breaking of the double hydrogen-bond in the system, while the molecular separation between two FA^+ is only slightly increased by the Coulomb force during this time.

Ultrafast intermolecular decay processes in a double hydrogen-bond dimer of formic acid (FA) molecules have been investigated using fragment ions and electron coincident momentum spectroscopy and also *ab initio* calculations. We observe direct evidence of ICD in the decay of formic acid dimer (FAD) ionized by electron impact (E_0 = 90 eV). First, the back-to-back emission of ion pairs reveals a two-body dissociation property of the fragmenting dicationic dimers. Second, the measurements of projectile energy loss distributions in coincidence with the ion pair indicate that the reaction is initiated by removal of an electron from the inner-valence (oxygen 2s) shell of the FA molecule, while a sequential process in which the projectile ionizes one molecule after the other is only a minor channel here. Third, the measured electron spectra provide an important signature of the decay process, i.e., the enhancement of low-energy (<10 eV) ICD electrons in comparison with the ionization spectrum of isolated FA molecules. Furthermore, the intermolecular proton transfer is not identified in the present experiments,[12,16,53] e.g., $[FA - H]^+ + [FA + H]^+$ channel, supporting that ICD is a very efficient process taking place before the proton transfer.

This ultrafast mechanism forms a dicationic dimer with two charges located at each of the two molecules, leading typically to a Coulomb explosion of the system. The fragmentation dynamics of $FA^+\cdots FA^+$ dications were interpreted with the help of AIMD simulations showing that the measured KER spectrum of $FA^+ + FA^+$ ion pair is very well reproduced only when starting from a planar eight-membered ring structure of the neutral dimer, while the other isomers are found to be minor contributions to the present supersonic gas experiment. Furthermore, our study reveals a fast and concerted breaking of the double hydrogen-bond initiated by the strong rotational motions of two FA^+ cations following the intermolecular decay mechanism and thus discloses a potential role of ultrafast molecular rotation in breaking the intermolecular hydrogen-bonds. The present study of ICD in formic acid dimers is expected to be relevant in radiation damage of biological tissues, both for the fundamental reason for generating genotoxic particles (low-energy electrons and radicals) and because of the double hydrogen-bond breakage induced by this ultrafast decay process. Indeed, our further calculations indicate that it may also occur in the hydrogen-bonding adenine−thymine and guanine−cytosine base pairs, where the computed double ionization thresholds are 18.6 and 18.3 eV, respectively, at the CCSD(T)/cc-pVDZ level. These threshold values are much lower than for FAD, suggesting that ICD is energetically accessible for DNA base pairs.

■ METHODS

Experimental Methods. The experimental data were obtained by crossing an electron projectile beam with a gas target jet and employing a multiparticle coincidence spectrometer (reaction microscope) for detection of the charged collision fragments.[43,45] The formic acid dimers are generated in a supersonic expansion of helium gas (stagnation pressure 1 bar) with seeded formic acid vapor. The pulsed electron beam is produced in an electron gun from a tantalum photocathode which is irradiated by UV-light pulses of 0.5 ns duration, and it is collimated by electrostatic lens elements. The energy width of the electron beam is about 0.5 eV.[44] It is guided by an axial magnetic field (0.7 mT) to the crossing zone with the gas jet and further to a beam dump which is a central bore in the electron detector. Secondary electrons and ions are extracted by means of a homogeneous electric field to opposite directions and projected onto two position- and time-sensitive multichannel plate detectors with 80 mm diameter of the active area. From the impact positions and the times-of-flight the momentum vectors and consequently the kinetic energies of the particles emerging from the reaction are determined. The acceptance angle for detection of low energy electrons up to the kinetic energy of 15 eV is almost 4π with the exception of small forward and backward angles which are lost due to the detector bore. In order to maximize the acceptance for molecular ion fragments, the electric extraction field of 1.0 V cm^{-1} is ramped up to 20 V cm^{-1} after 400 ns when the electrons have reached the detector. In our experiment, monomer ionization is simultaneously recorded with cluster ionization.

The absolute cross section for SI leading to $FA^+ + FA^+$ ion pair is calculated by multiplying the partial ionization cross section for the first collision partner with the probability to subsequently ionize the second molecule. The latter is the relative size of its ionization cross section compared to the total surface area of a sphere with radius of the intermolecular distance. The calculations can be expressed as following:

$$\sigma_{SI}(E_0) = \sigma^+_{FA}(E_0)\frac{\sigma^+_{FA}(E_1)}{4\pi R^2} \quad (1)$$

Here $\sigma^+_{FA}(E_0 = 90\text{ eV}) \approx \sigma^+_{FA}(E_1 = 78.5\text{ eV}) \approx 1.0\ \text{Å}^2$ is the partial ionization cross section for production of FA^+ at the projectile energy of E_0 = 90 eV and E_1 = 78.5 eV which considers the minimum energy loss in the first collision.[54] R = 3.0 Å is the intermolecular center-of-mass distance obtained from the molecular geometry calculations.[46] As a result, we obtain $\sigma_{SI}(90\text{ eV}) \approx 0.885 \times 10^{-18}\ cm^2$. The oxygen 2s (O2s)

https://doi.org/10.1021/acs.jpclett.2c00957
J. Phys. Chem. Lett. 2022, 13, 4272−4279

ionization cross section of FA molecule is not available in the literature, we refer to a value of about 1.73×10^{-17} cm^2 for the O2s ionization of water.[33] This indicates that SI in the formic acid dimer is only a minor channel in comparison to O2s inner-valence ionization of molecules.

Computational Methods. The double ionization thresholds of formic acid dimer (28.45 eV) and monomer (33.24 eV) were obtained at the EOM-DIP-CCSD/cc-pVDZ level of theory with the nonelectron-conserving variant of EOM-CCSD where target states are reached by detaching two electrons from the corresponding ground state.[55,56] The calculations were performed using the Q-Chem 4.2 program suite.[57]

We performed calculations for the fragmentation dynamics of the $FA^+\cdots FA^+$ dication on the electronic ground state. In these calculations, we considered six lowest energy isomers of the formic acid (FA) dimers (Figure 4) including the planar eight-membered ring structure that corresponds to the global energy minimum geometry.[46] The AIMD simulations were performed in two steps: (i) the initial conditions, i.e., geometries and velocities of every atom, of neutral $(FA)_2$ were sampled by the quasi-classical fixed normal-mode sampling method[58] under the temperature of about 30 K in which the populations of the initial vibrational states were determined by Boltzmann distributions; (ii) we assumed an instantaneous vertical transition to the electronic ground state of the doubly charged $FA^+ \cdots FA^+$ dimer. The molecular dynamics simulation was performed under the extended Lagrangian molecular dynamics scheme adopting the so-called atom-centered density matrix propagation (ADMP) method[58−60] using the long-ranged density-functional theory method at the ωB97XD/cc-pVTZ level. We obtained the dynamical simulations for 500 fs time range with 0.5 fs time step under the approximate self-consistent field convergence at each time step. This method enables Born−Oppenheimer molecular dynamics on a given electronic state with accurate long-term energy conservation. All calculations were carried out with the Gaussian 16 suite of programs.[61]

The vertical ionization spectrum of FAD was computed using the third-order algebraic diagrammatic construction (ADC(3)) approximation scheme for the one-particle Green's function.[62−65] The ADC(3) method describes the energies and pole strengths of ionization transitions involving the "one-hole" (1h) and "two-hole−one-particle" (2h−1p) electronic states through third and first order, respectively, in the residual electronic interaction. The ADC(3) eigenstate equations[66] are solved using the Block−Lanczos procedure which is applicable in situations where the breakdown of the orbital picture of ionization[67] takes place. The latter phenomenon manifests itself by a strong redistribution of spectral intensity from the 1h main states to 2h−1p satellites and is typical for inner-valence ionization considered in this work. The ADC(3) method was previously applied in various molecules including computations of ionization spectra of the valence,[68−70] inner-valence,[71] and K-shell[72] orbitals and is proved to be an accurate and valuable tool in spectroscopic studies. The cc-pVTZ basis set was used in the calculations. The resulting spectral envelopes (constructed by convolving the generated spectra with Gaussians of the fwhm (full width at half-maximum) equal to 0.2 eV) are shown in Figure 3e together with the underlying transitions, which are presented by the black lines. The contributions of the inner-valence O2s holes are presented by the colored envelopes in the energy region from 25 to 40 eV.

■ ASSOCIATED CONTENT

Supporting Information

The Supporting Information is available free of charge at https://pubs.acs.org/doi/10.1021/acs.jpclett.2c00957.

Detailed description of the single ionization spectra of FAD in the $O2s^{-1}$ energy region, calculated initial Coulomb energy of $FA^+ + FA^+$ channel, and calculated ICD electron spectrum (PDF)

Animated movie for the Coulomb explosion process (AVI)

■ AUTHOR INFORMATION

Corresponding Author

Xueguang Ren − *School of Physics, Xi'an Jiaotong University, Xi'an 710049, China; Max-Planck-Institut für Kernphysik, Heidelberg 69117, Germany;* orcid.org/0000-0001-6132-092X; Email: renxueguang@xjtu.edu.cn

Authors

Jiaqi Zhou − *School of Physics, Xi'an Jiaotong University, Xi'an 710049, China; Max-Planck-Institut für Kernphysik, Heidelberg 69117, Germany*

Shaokui Jia − *School of Physics, Xi'an Jiaotong University, Xi'an 710049, China*

Anna D. Skitnevskaya − *Laboratory of Quantum Chemistry, Irkutsk State University, Irkutsk 664003, Russia; Theoretische Chemie, Physikalisch-Chemisches Institut, Universität Heidelberg, Heidelberg 69120, Germany;* orcid.org/0000-0002-9328-1598

Enliang Wang − *Max-Planck-Institut für Kernphysik, Heidelberg 69117, Germany; J. R. Macdonald Laboratory, Department of Physics, Kansas State University, Manhattan, Kansas 66506, United States;* orcid.org/0000-0002-5703-6501

Theresa Hähnel − *Theoretische Chemie, Physikalisch-Chemisches Institut, Universität Heidelberg, Heidelberg 69120, Germany*

Emma K. Grigoricheva − *Laboratory of Quantum Chemistry, Irkutsk State University, Irkutsk 664003, Russia; Theoretische Chemie, Physikalisch-Chemisches Institut, Universität Heidelberg, Heidelberg 69120, Germany*

Xiaorui Xue − *School of Physics, Xi'an Jiaotong University, Xi'an 710049, China*

Jian-Xing Li − *School of Physics, Xi'an Jiaotong University, Xi'an 710049, China*

Alexander I. Kuleff − *Theoretische Chemie, Physikalisch-Chemisches Institut, Universität Heidelberg, Heidelberg 69120, Germany*

Alexander Dorn − *Max-Planck-Institut für Kernphysik, Heidelberg 69117, Germany;* orcid.org/0000-0002-8024-224X

Complete contact information is available at: https://pubs.acs.org/10.1021/acs.jpclett.2c00957

Notes

The authors declare no competing financial interest.

■ ACKNOWLEDGMENTS

The authors are grateful to Prof. L. S. Cederbaum, Dr. K. Gokhberg, and Prof. A. B. Trofimov for helpful discussions. This work was supported by the National Natural Science Foundation of China under Grants 11974272 and 11774281

and by the Deutsche Forschungsgemeinschaft (DFG) under Project RE 2966/5-1. A.D.S. and E.K.G. acknowledge Grant FZZE-2020-0025 from the Ministry of Science and Higher Education of the Russian Federation. A.I.K. acknowledges the financial support by the European Research Council (ERC) (Advanced Investigator Grant 692657). J.Z. is grateful for the support from the China Scholarship Council (CSC). E.W. acknowledges a fellowship from the Alexander von Humboldt Foundation.

■ REFERENCES

(1) Mahadevi, A. S.; Sastry, G. N. Cooperativity in Noncovalent Interactions. *Chem. Rev.* **2016**, *116*, 2775−2825.
(2) Hobza, P.; Havlas, Z. Blue-Shifting Hydrogen Bonds. *Chem. Rev.* **2000**, *100*, 4253−4264.
(3) Hobza, P. Theoretical studies of hydrogen bonding. *Annu. Rep. Prog. Chem., Sect. C: Phys. Chem.* **2004**, *100*, 3−27.
(4) Jeffrey, G. A.; Saenger, W. *Hydrogen Bonding in Biological Structures*; Springer: Berlin, 1991.
(5) Laage, D.; Elsaesser, T.; Hynes, J. T. Water Dynamics in the Hydration Shells of Biomolecules. *Chem. Rev.* **2017**, *117*, 10694−10725.
(6) Richardson, J. O.; Pérez, C.; Lobsiger, S.; Reid, A. A.; Temelso, B.; Shields, G. C.; Kisiel, Z.; Wales, D. J.; Pate, B. H.; Althorpe, S. C. Concerted hydrogen-bond breaking by quantum tunneling in the water hexamer prism. *Science* **2016**, *351*, 1310.
(7) Zhao, G.-J.; Han, K.-L. Hydrogen Bonding in the Electronic Excited State. *Acc. Chem. Res.* **2012**, *45*, 404−413.
(8) Golan, A.; Bravaya, K. B.; Kudirka, R.; Kostko, O.; Leone, S. R.; Krylov, A. I.; Ahmed, M. Ionization of dimethyluracil dimers leads to facile proton transfer in the absence of hydrogen bonds. *Nat. Chem.* **2012**, *4*, 323−329.
(9) Wang, E.; Ren, X.; Baek, W.; Rabus, H.; Pfeifer, T.; Dorn, A. Water acting as a catalyst for electron-driven molecular break-up of tetrahydrofuran. *Nat. Commun.* **2020**, *11*, 2194.
(10) Allan, M. Electron Collisions with Formic Acid Monomer and Dimer. *Phys. Rev. Lett.* **2007**, *98*, 123201.
(11) Matylitsky, V. V.; Riehn, C.; Gelin, M. F.; Brutschy, B. The formic acid dimer $(HCOOH)_2$ probed by time-resolved structure selective spectroscopy. *J. Chem. Phys.* **2003**, *119*, 10553−10562.
(12) Birer, Ö.; Havenith, M. High-Resolution Infrared Spectroscopy of the Formic Acid Dimer. *Annu. Rev. Phys. Chem.* **2009**, *60*, 263−275.
(13) Scheiner, S.; Kern, C. W. Molecular orbital investigation of multiply hydrogen bonded systems. Formic acid dimer and DNA base pairs. *J. Am. Chem. Soc.* **1979**, *101*, 4081−4085.
(14) Hoshina, K.; Hagihara, H.; Tsuge, M. Double Ionization and Coulomb Explosion of the Formic Acid Dimer by Intense Near-Infrared Femtosecond Laser Pulses. *J. Phys. Chem. A* **2012**, *116*, 826−831.
(15) Novak, J.; Mališ, M.; Prlj, A.; Ljubić, I.; Kühn, O.; Došlić, N. Photoinduced Dynamics of Formic Acid Monomers and Dimers: The Role of the Double Hydrogen Bond. *J. Phys. Chem. A* **2012**, *116*, 11467−11475.
(16) Farfán, P.; Echeverri, A.; Diaz, E.; Tapia, J. D.; Gómez, S.; Restrepo, A. Dimers of formic acid: Structures, stability, and double proton transfer. *J. Chem. Phys.* **2017**, *147*, 044312.
(17) Arruda, M. S.; Medina, A.; Sousa, J. N.; Mendes, L. A. V.; Marinho, R. R. T.; Prudente, F. V. Communication: Protonation process of formic acid from the ionization and fragmentation of dimers induced by synchrotron radiation in the valence region. *J. Chem. Phys.* **2016**, *144*, 141101.
(18) Cederbaum, L. S.; Zobeley, J.; Tarantelli, F. Giant Intermolecular Decay and Fragmentation of Clusters. *Phys. Rev. Lett.* **1997**, *79*, 4778−4781.
(19) Kuleff, A. I.; Cederbaum, L. S. Tracing Ultrafast Interatomic Electronic Decay Processes in Real Time and Space. *Phys. Rev. Lett.* **2007**, *98*, 083201.
(20) Schnorr, K.; et al. Time-Resolved Measurement of Interatomic Coulombic Decay in Ne_2. *Phys. Rev. Lett.* **2013**, *111*, 093402.
(21) Trinter, F.; et al. Evolution of Interatomic Coulombic Decay in the Time Domain. *Phys. Rev. Lett.* **2013**, *111*, 093401.
(22) Hergenhahn, U. Interatomic and intermolecular coulombic decay: The early years. *J. Electron Spectrosc. Relat. Phenom.* **2011**, *184*, 78−90.
(23) Jahnke, T.; Hergenhahn, U.; Winter, B.; Dörner, R.; Frühling, U.; Demekhin, P. V.; Gokhberg, K.; Cederbaum, L. S.; Ehresmann, A.; Knie, A.; Dreuw, A. Interatomic and Intermolecular Coulombic Decay. *Chem. Rev.* **2020**, *120*, 11295−11369.
(24) Sisourat, N.; Kryzhevoi, N. V.; Kolorenč, P.; Scheit, S.; Jahnke, T.; Cederbaum, L. S. Ultralong-range energy transfer by interatomic Coulombic decay in an extreme quantum system. *Nat. Phys.* **2010**, *6*, 508−511.
(25) Nagaya, K.; et al. Interatomic Coulombic decay cascades in multiply excited neon clusters. *Nat. Commun.* **2016**, *7*, 13477.
(26) Trinter, F.; et al. Resonant Auger decay driving intermolecular Coulombic decay in molecular dimers. *Nature* **2014**, *505*, 664−666.
(27) O'Keeffe, P.; Ripani, E.; Bolognesi, P.; Coreno, M.; Devetta, M.; Callegari, C.; Di Fraia, M.; Prince, K. C.; Richter, R.; Alagia, M.; Kivimäki, A.; Avaldi, L. The Role of the Partner Atom and Resonant Excitation Energy in Interatomic Coulombic Decay in Rare Gas Dimers. *J. Phys. Chem. Lett.* **2013**, *4*, 1797−1801.
(28) Iskandar, W.; et al. Tracing intermolecular Coulombic decay of carbon-dioxide dimers and oxygen dimers after valence photo-ionization. *Phys. Rev. A* **2019**, *99*, 043414.
(29) Jahnke, T.; et al. Ultrafast energy transfer between water molecules. *Nat. Phys.* **2010**, *6*, 139−142.
(30) Mucke, M.; Braune, M.; Barth, S.; Forstel, M.; Lischke, T.; Ulrich, V.; Arion, T.; Becker, U.; Bradshaw, A.; Hergenhahn, U. A hitherto unrecognized source of low-energy electrons in water. *Nat. Phys.* **2010**, *6*, 143−146.
(31) Richter, C.; Hollas, D.; Saak, C.-M.; Förstel, M.; Miteva, T.; Mucke, M.; Björneholm, O.; Sisourat, N.; Slavíček, P.; Hergenhahn, U. Competition between proton transfer and intermolecular Coulombic decay in water. *Nat. Commun.* **2018**, *9*, 4988.
(32) Stoychev, S. D.; Kuleff, A. I.; Cederbaum, L. S. Intermolecular Coulombic Decay in Small Biochemically Relevant Hydrogen-Bonded Systems. *J. Am. Chem. Soc.* **2011**, *133*, 6817−6824.
(33) Ren, X.; Wang, E.; Skitnevskaya, A. D.; Trofimov, A. B.; Gokhberg, K.; Dorn, A. Experimental evidence for ultrafast intermolecular relaxation processes in hydrated biomolecules. *Nat. Phys.* **2018**, *14*, 1062−1066.
(34) Obaid, R.; Xiong, H.; Augustin, S.; Schnorr, K.; Ablikim, U.; Battistoni, A.; Wolf, T. J. A.; Bilodeau, R. C.; Osipov, T.; Gokhberg, K.; Rolles, D.; LaForge, A. C.; Berrah, N. Intermolecular Coulombic Decay in Endohedral Fullerene at the $4d \rightarrow 4f$ Resonance. *Phys. Rev. Lett.* **2020**, *124*, 113002.
(35) LaForge, A. C.; Shcherbinin, M.; Stienkemeier, F.; Richter, R.; Moshammer, R.; Pfeifer, T.; Mudrich, M. Highly efficient double ionization of mixed alkali dimers by intermolecular Coulombic decay. *Nat. Phys.* **2019**, *15*, 247−250.
(36) Ren, X.; Zhou, J.; Wang, E.; Yang, T.; Xu, Z.; Sisourat, N.; Pfeifer, T.; Dorn, A. Ultrafast energy transfer between π-stacked aromatic rings upon inner-valence ionization. *Nat. Chem.* **2022**, *14*, 232−238.
(37) Thürmer, S.; Oncak, M.; Ottosson, N.; Seidel, R.; Hergenhahn, U.; Bradforth, S. E.; Slavicek, P.; Winter, B. On the nature and origin of dicationic, charge-separated species formed in liquid water on X-ray irradiation. *Nat. Chem.* **2013**, *5*, 590−596.
(38) Slavíček, P.; Winter, B.; Cederbaum, L. S.; Kryzhevoi, N. V. Proton-Transfer Mediated Enhancement of Nonlocal Electronic Relaxation Processes in X-ray Irradiated Liquid Water. *J. Am. Chem. Soc.* **2014**, *136*, 18170−18176.
(39) Grieves, G. A.; Orlando, T. M. Intermolecular Coulomb Decay at Weakly Coupled Heterogeneous Interfaces. *Phys. Rev. Lett.* **2011**, *107*, 016104.

https://doi.org/10.1021/acs.jpclett.2c00957
J. Phys. Chem. Lett. 2022, 13, 4272−4279

(40) Pimblott, S. M.; LaVerne, J. A. Production of low-energy electrons by ionizing radiation. *Radiat. Phys. Chem.* **2007**, *76*, 1244−1247.
(41) Garrett, B. C.; et al. Role of Water in Electron-Initiated Processes and Radical Chemistry: Issues and Scientific Advances. *Chem. Rev.* **2005**, *105*, 355−390.
(42) Alizadeh, E.; Orlando, T. M.; Sanche, L. Biomolecular Damage Induced by Ionizing Radiation: The Direct and Indirect Effects of Low-Energy Electrons on DNA. *Annu. Rev. Phys. Chem.* **2015**, *66*, 379−398.
(43) Ullrich, J.; Moshammer, R.; Dorn, A.; Dörner, R.; Schmidt, L.; Schmidt-Böcking, H. Recoil-ion and electron momentum spectroscopy: reaction-microscopes. *Rep. Prog. Phys.* **2003**, *66*, 1463.
(44) Ren, X.; Pflüger, T.; Weyland, M.; Baek, W. Y.; Rabus, H.; Ullrich, J.; Dorn, A. An (e, 2e + ion) study of low-energy electron-impact ionization and fragmentation of tetrahydrofuran with high mass and energy resolutions. *J. Chem. Phys.* **2014**, *141*, 134314.
(45) Ren, X.; Jabbour Al Maalouf, E.; Dorn, A.; Denifl, S. Direct evidence of two interatomic relaxation mechanisms in argon dimers ionized by electron impact. *Nat. Commun.* **2016**, *7*, 11093.
(46) Chocholoušová, J.; Vacek, J.; Hobza, P. Potential energy and free energy surfaces of the formic acid dimer: Correlated ab initio calculations and molecular dynamics simulations. *Phys. Chem. Chem. Phys.* **2002**, *4*, 2119−2122.
(47) Potts, A. W.; Williams, T. A.; Price, W. C. Ultra-violet photoelectron data on the complete valence shells of molecules recorded using filtered 30.4 nm radiation. *Faraday Discuss. Chem. Soc.* **1972**, *54*, 104−115.
(48) Schirmer, J.; Cederbaum, L. S.; Domcke, W.; Von Niessen, W. Complete breakdown of the quasiparticle picture for inner-valence electrons: Hydrogen cyanide and formic acid. *Chem. Phys. Lett.* **1978**, *57*, 582−587.
(49) von Niessen, W.; Bieri, G.; Åsbrink, L. 30.4-nm He (II) photoelectron spectra of organic molecules: Part III. Oxo-compounds (C, H, O). *J. Electron Spectrosc. Relat. Phenom.* **1980**, *21*, 175−191.
(50) Bharathi, S. M.; Datta, S. K.; Grisogono, A. M.; Pascual, R.; Weigold, E.; von Niessen, W. Investigation of the complete valence shell of formic acid by electron momentum spectroscopy and Green's function methods. *J. Electron Spectrosc. Relat. Phenom.* **1990**, *53*, 51−78.
(51) Vendrell, O.; Stoychev, S. D.; Cederbaum, L. S. Generation of Highly Damaging H_2O^+ Radicals by Inner Valence Shell Ionization of Water. *ChemPhysChem* **2010**, *11*, 1006−1009.
(52) Zhou, J.; He, C.; Liu, M.-M.; Wang, E.; Jia, S.; Dorn, A.; Ren, X.; Liu, Y. Real-time observation of ultrafast molecular rotation in weakly bound dimers. *Phys. Rev. Research* **2021**, *3*, 023050.
(53) Tachikawa, H. Proton Transfer vs Complex Formation Channels in Ionized Formic Acid Dimer: A Direct Ab Initio Molecular Dynamics Study. *J. Phys. Chem. A* **2020**, *124*, 3048−3054.
(54) Zawadzki, M. Electron-impact ionization cross section of formic acid. *Eur. Phys. J. D* **2018**, *72*, 12.
(55) Kuś, T.; Krylov, A. I. Using the charge-stabilization technique in the double ionization potential equation-of-motion calculations with dianion references. *J. Chem. Phys.* **2011**, *135*, 084109.
(56) Kuś, T.; Krylov, A. I. De-perturbative corrections for charge-stabilized double ionization potential equation-of-motion coupled-cluster method. *J. Chem. Phys.* **2012**, *136*, 244109.
(57) Shao, Y.; et al. Advances in molecular quantum chemistry contained in the Q-Chem 4 program package. *Mol. Phys.* **2015**, *113*, 184−215.
(58) Schlegel, H. B.; Millam, J. M.; Iyengar, S. S.; Voth, G. A.; Daniels, A. D.; Scuseria, G. E.; Frisch, M. J. Ab initio molecular dynamics: Propagating the density matrix with Gaussian orbitals. *J. Chem. Phys.* **2001**, *114*, 9758−9763.
(59) Iyengar, S. S.; Schlegel, H. B.; Millam, J. M.; Voth, G. A.; Scuseria, G. E.; Frisch, M. J. Ab initio molecular dynamics: Propagating the density matrix with Gaussian orbitals. II. Generalizations based on mass-weighting, idempotency, energy conservation and choice of initial conditions. *J. Chem. Phys.* **2001**, *115*, 10291−10302.
(60) Schlegel, H. B.; Iyengar, S. S.; Li, X.; Millam, J. M.; Voth, G. A.; Scuseria, G. E.; Frisch, M. J. Ab initio molecular dynamics: Propagating the density matrix with Gaussian orbitals. III. Comparison with Born−Oppenheimer dynamics. *J. Chem. Phys.* **2002**, *117*, 8694−8704.
(61) Frisch, M. J.; et al. *Gaussian 16*, revision A.03; Gaussian Inc.: Wallingford, CT, 2016.
(62) Schirmer, J.; Cederbaum, L. S.; Walter, O. New approach to the one-particle Green's function for finite Fermi systems. *Phys. Rev. A* **1983**, *28*, 1237−1259.
(63) Schirmer, J.; Angonoa, G. On Green's function calculations of the static self-energy part, the ground state energy and expectation values. *J. Chem. Phys.* **1989**, *91*, 1754−1761.
(64) von Niessen, W.; Schirmer, J.; Cederbaum, L. S. Computational methods for the one-particle greenas function. *Computer Physics Reports* **1984**, *1*, 57−125.
(65) Weikert, H. G.; Meyer, H. D.; Cederbaum, L. S.; Tarantelli, F. Block Lanczos and many-body theory: Application to the one-particle Green's function. *J. Chem. Phys.* **1996**, *104*, 7122−7138.
(66) Meyer, H. D.; Pal, S. A band-Lanczos method for computing matrix elements of a resolvent. *J. Chem. Phys.* **1989**, *91*, 6195−6204.
(67) Cederbaum, L. S.; Domcke, W.; Schirmer, J.; Niessen, W. V. *Advances in Chemical Physics*; John Wiley Sons, Ltd., 1986; Chapter 3, pp 115−159.
(68) Trofimov, A. B.; Holland, D. M. P.; Powis, I.; Menzies, R. C.; Potts, A. W.; Karlsson, L.; Gromov, E. V.; Badsyuk, I. L.; Schirmer, J. Ionization of pyridine: Interplay of orbital relaxation and electron correlation. *J. Chem. Phys.* **2017**, *146*, 244307.
(69) Duran, A. T.; Powis, I.; Holland, D. M. P.; Nicolas, C.; Bozek, J.; Trofimov, A. B.; Grigoricheva, E. K.; Skitnevskaya, A. D. Vibronic interaction in trans-dichloroethene studied by vibration- and angle-resolved photoelectron spectroscopy using 19-90 eV photon energy. *J. Chem. Phys.* **2021**, *154*, 094303.
(70) Patanen, M.; Abid, A. R.; Pratt, S. T.; Kivimäki, A.; Trofimov, A. B.; Skitnevskaya, A. D.; Grigoricheva, E. K.; Gromov, E. V.; Powis, I.; Holland, D. M. P. Valence shell photoelectron angular distributions and vibrationally resolved spectra of imidazole: A combined experimental-theoretical study. *J. Chem. Phys.* **2021**, *155*, 054304.
(71) Zobeley, J.; Cederbaum, L. S.; Tarantelli, F. Intermolecular Coulombic Decay of Molecular Clusters: Identification of the Decay Mechanism Using a New Hole-Population Analysis. *J. Phys. Chem. A* **1999**, *103*, 11145−11160.
(72) Plekan, O.; Feyer, V.; Richter, R.; Moise, A.; Coreno, M.; Prince, K. C.; Zaytseva, I. L.; Moskovskaya, T. E.; Soshnikov, D. Y.; Trofimov, A. B. X-ray Spectroscopy of Heterocyclic Biochemicals: Xanthine, Hypoxanthine, and Caffeine. *J. Phys. Chem. A* **2012**, *116*, 5653−5664.

https://doi.org/10.1021/acs.jpclett.2c00957
J. Phys. Chem. Lett. 2022, 13, 4272−4279